Journal of Environmental Management 345 (2023) 118736

Contents lists available at ScienceDirect

Journal of Environmental Management

journal homepage: www.elsevier.com/locate/jenvman

Research article

Combining Landsat time series and GEDI data for improved characterization of fuel types and canopy metrics in wildfire simulation

Viktor Myroniuk [a,*], Sergiy Zibtsev [a,b], Vadym Bogomolov [c], Johann Georg Goldammer [d], Oleksandr Soshenskyi [a], Viacheslav Levchenko [a], Maksym Matsala [a,e]

[a] National University of Life and Environmental Sciences of Ukraine, 15 Heroiv Oborony St., Kyiv, 03041, Ukraine
[b] Regional Eastern Europe Fire Monitoring Center, 8 Buchmy St., Office 250, Kyiv, 02152, Ukraine
[c] Ukrainian Research Institute of Forestry and Forest Melioration, 86 Pushkinska St., Kharkiv, 61024, Ukraine
[d] Max Planck Institute for Chemistry and Freiburg University, Global Fire Monitoring Center, 75 Georges-Köhler-Allee, Freiburg, 79110, Germany
[e] Swedish University of Agricultural Sciences, Southern Swedish Forest Research Centre, Box 190, 234 22, Lomma, Alnarp, Sweden

ARTICLE INFO

Handling Editor: Lixiao Zhang

Keywords:
Fire behavior
Temporal segmentation
Stand height
Canopy density
Imputation
CCDC

ABSTRACT

Wildfires in the Chornobyl Exclusion Zone (CEZ) and other radioactively contaminated areas threaten human health and well-being with the potential to resuspend radionuclides. Wildfire behavior simulation is a necessary tool to examine the efficiency of fuel treatments in the CEZ, but it requires systematically updated maps of fuel types and canopy metrics. The objective of this study was to demonstrate an effective approach for mapping fuel types, canopy height (CH), and canopy cover (CC) in territories contaminated by radionuclides using Landsat time series (LTS) and Global Ecosystem Dynamics Investigation (GEDI) LiDAR observations. We combined LTS and GEDI data to map fuel types and canopy metrics used in wildfire simulations within the CEZ. Our classification model showed an adequate overall accuracy (75%) in mapping land covers and associated fuel types. The phenology metrics extracted from LTS reliably distinguished spectrally similar vegetation types (such as grasslands and croplands) which exhibit different flammability through the year. We also predicted a suite of relative heights metrics and CC at Landsat 30-m pixel level (R^2 = 0.23–0.26) using the nearest neighbor technique. The imputed maps adequately captured the dynamics of CH and CC in the CEZ after recent large wildfires occurred in 2015, 2020, and 2022. Thus, we illustrate a LTS processing approach to produce wall-to-wall maps of canopy characteristics that are important for wildfire simulations. We conclude that continuous updating of land cover and canopy fuel data is crucial to ensure relevant fire management of radioactively contaminated landscapes and support local decision-making.

1. Introduction

Wildfires in areas contaminated after the Chornobyl Nuclear Power Plant (CNPP) accident in 1986 represent a significant problem due to the risk of the radionuclides resuspension (Evangeliou et al., 2016), and consequent exposure of firefighters to radioactive contamination (Kashparov et al., 2015). The Chornobyl Exclusion Zone (CEZ), which covers approximately 260,000 ha of hazardous areas in Ukraine, has attracted the attention of the international community due to the most recent wildfires. Two fires in 2015 (15,000 ha), and in 2020 (66,000 ha) burned about one third of the region's territory (Evangeliou et al., 2016; Fedoniuk et al., 2021). Human-caused ignitions (e.g., vehicles, machinery, negligence, and other accidental causes) have been common within the CEZ. Ignited fires on grasslands during dry and windy conditions spread towards the CEZ. To address these potential harms, comprehensive information about vegetation properties and wildfire fuels can support preventive programs for wildfire risk management (Reeves et al., 2009). The growing incidence of large fires across the CEZ during the last decade motivated an investigation that used wildfire simulation approaches to explore fire risk (Ager et al., 2019). Specifically, the analysis of fire risk revealed a higher likelihood of ignitions in areas with a predominance of grassy fuels. The fire spread component was mostly associated with the specific distribution pattern of grasslands and fire-prone pine plantations. Further methodological and technical advances are required to develop effective and easy-to-use decision support tools that utilize wildfire modeling outputs (Kalabokidis et al.,

* Corresponding author.
E-mail address: victor.myroniuk@nubip.edu.ua (V. Myroniuk).

https://doi.org/10.1016/j.jenvman.2023.118736
Received 18 December 2022; Received in revised form 24 July 2023; Accepted 30 July 2023

2016; Myroniuk et al., 2021).

Realistic wildfire simulation at the landscape level relies on spatially accurate information about fuel continuity. As long as fuel maps are essential for modeling, standardized and cost-effective methods for updating these maps are required (Rollins et al., 2004). Unlike in other countries in Europe where the fuel layers can be seamlessly compiled using available land cover or land use maps (Alcasena et al., 2017; Salis et al., 2021), such geospatial data sets do not exist for many areas in Ukraine. Therefore, remote sensing-based approaches are promising for characterizing fuel properties in a fine spatial and temporal domain. Many recent studies utilized satellite imagery for mapping fuel types to model fire behavior at regional to national scales (Aragoneses and Chuvieco, 2021; Stefanidou et al., 2020b). Remote sensing can be an effective method for updating information on hard-to-reach areas such as those contaminated by radionuclides and, since 2022, by unexploded ordnance (UXO) and land mines where field data collection may be restricted or limited due to risks to human life (Matsala et al., 2021a).

Satellite time series offer excellent opportunities to characterize the dynamic nature of vegetation properties affecting the distribution of fuels across the landscape. Transitions between land cover types can be efficiently mapped using temporal segmentation algorithms that utilize fitted trajectories of spectral data for multi-date classification (Zhu, 2017). Unlike many algorithms that are mostly focused on detection of annual vegetation changes, the Continuous Change Detection and Classification (CCDC) approach (Zhu and Woodcock, 2014) has advantages in mapping fuels. In addition to direct classification of trajectories, the CCDC provides valuable information on vegetation phenology that can improve fuel classification in accordance with the cyclic patterns of spectral reflectance throughout the year.

Optical satellite data are more commonly utilized to map fuel types (Aragoneses and Chuvieco, 2021), however, active remote sensing is preferred to quantify the fuel load (Mutlu et al., 2008) or canopy fuels (Andersen et al., 2005; Maltamo et al., 2020) as it directly interacts with the vertical structure of vegetation. In particular, canopy vertical profile metrics such as canopy height (CH) and canopy base height (CBH) can be accurately retrieved using the LiDAR technology (Andersen et al., 2005; Stefanidou et al., 2020a). Nevertheless, to scale collected LiDAR data from local to regional or national levels, covariates from optical satellite imagery and predictive mapping are required (Chuvieco et al., 2020; Wilkes et al., 2015). For example, Moran et al. (2020) highlighted the utility of the LiDAR-Landsat fusion in various landscapes over the western US to predict canopy fuels.

When resources for collection of the airborne laser scanning data are limited, the NASA Global Ecosystem Dynamics Investigation (GEDI) spaceborne LiDAR sensor is very promising for large-scale evaluation of vegetation structural parameters. After the launch of the GEDI system, a number of its applications were reported to map forest attributes (Fayad et al., 2021; Rishmawi et al., 2021a), aboveground biomass (Dubayah et al., 2022), and vegetation types (Dwiputra et al., 2023). The full waveform GEDI metrics were effectively used to map CH in various regions of the world (Dorado-Roda et al., 2021; Francini et al., 2022; Rishmawi et al., 2021a). Potapov et al. (2021) demonstrated the potential for integrating GEDI data and Landsat time series (LTS) for nearly global mapping of CH and its dynamics. Despite the considerable focus on GEDI data in various forest programs, the issue of monitoring fuel characteristics for wildfire simulation has not been discussed in detail. Nevertheless, GEDI footprint-level variables are very promising for forest fuel modeling (Hoffrén et al., 2023). Leite et al. (2022) demonstrated a framework for large-scale multi-layer fuel loads estimation in a Brazilian tropical savanna that can be scaled to other fire-prone areas. Thus, GEDI LiDAR observations can also improve characterization of fuels in wildfire studies.

Various machine learning approaches have been examined to predict forest structural attributes using GEDI data. Deep learning has proven to be effective for handling raw LiDAR waveforms at the footprint level. Fayad et al. (2021) demonstrated that a metric-free convolutional neural network provides reliable predictions of canopy height and wood volume. However, metric-based approaches have become more common for forest fuel classification using GEDI observations (Hoffrén et al., 2023; Leite et al., 2022). The GEDI products have limitations in displaying wall-to-wall landscape features. Thus, propagations of footprint-level forest structure metrics over a larger geographical areas has been a major concern in numerous studies (Healey et al., 2020; Rishmawi et al., 2021b; Wang et al., 2022). Previous investigations demonstrated that random forest (RF) models could provide reliable results for many practical applications. In addition to this and other ensemble machine learning algorithms (Shendryk, 2022), nearest neighbor imputation techniques have not yet been presented. However, multivariate imputation techniques (Moeur and Stage, 1995; Ohmann and Gregory, 2002) might be suitable for simultaneously processing a set of canopy metrics obtained at footprints and creating corresponding maps.

This study aims to develop an approach for updating fuels data in wildfire simulation using freely available LTS and GEDI data. Considering that field data collection within areas contaminated by radionuclides after the CNPP accident is always limited due to the risk to human life, there is a need for an accurate and cost-effective fuel mapping method. The specific focus of the manuscript is twofold: 1) to integrate GEDI data into existing nearest neighbor imputation workflows based on multispectral imagery in order to support fire behavior modeling, and 2) to characterize the decadal changes in distribution of fuel types within the CEZ due to major wildfires in 2015, 2020, and 2022.

2. Materials and methods

2.1. Study area

This study was performed in the area of the CEZ to extend the investigation of the wildfire problem in territories contaminated by radionuclides started by Ager et al. (2019). The current paper adds to that work by providing an effective tool for updating the fuel characteristics in a wider timeframe. More than half of the area is covered by forests, with prominence of Scots pine (*Pinus sylvestris* L.), along with mixed hardwood stands of silver birch (*Betula pendula* L.), black alder (*Alnus glutinosa* (L.) Gaertn.), common aspen (*Populus tremula* L.), and common oak (*Querqus robur* L.). The forests remain mostly unmanaged after the accident on the CNPP in 1986, with limited logging activities associated with the construction of facilities for nuclear waste disposal, salvage logging, and fuel treatments (fuelbreaks). Agricultural lands within the CEZ have been abandoned and have transitioned into natural meadows or mixed forests (Matsala et al., 2021a). In contrast, farmlands outside the CEZ boundaries are still used by farmers and the local population for crops production. Large wildfires that altered the spatial patterns of land cover and fuel distribution occurred within the CEZ in 1992, 2007, 2015, 2020, and 2022 (Matsala et al., 2021b). Field burning practice in areas that surrounds the CEZ has been among the major causes of wildfires on this area. Thus, we extended the study area beyond the contaminated sites within a nearly squared bounding box (123.78 × 133.50 km) in order to measure the effect of wildfire transmission from the outside and to improve representation of some rare land cover categories in the reference data set we collected for the classification (Fig. 1).

2.2. Data

2.2.1. Landsat time series

In our mapping approach, we used Landsat Collection 2 surface reflectance data (Landsat 5, Landsat 8, and Landsat 9) that was collected between January 1, 2010 and November 1, 2022. To eliminate the effect of Landsat 7 scan-line corrector failure that had an impact on the quality of the image collection between 2010 and 2013 (i.e., when only Landsat 5 and Landsat 7 are available), we decided to exclude the data of this

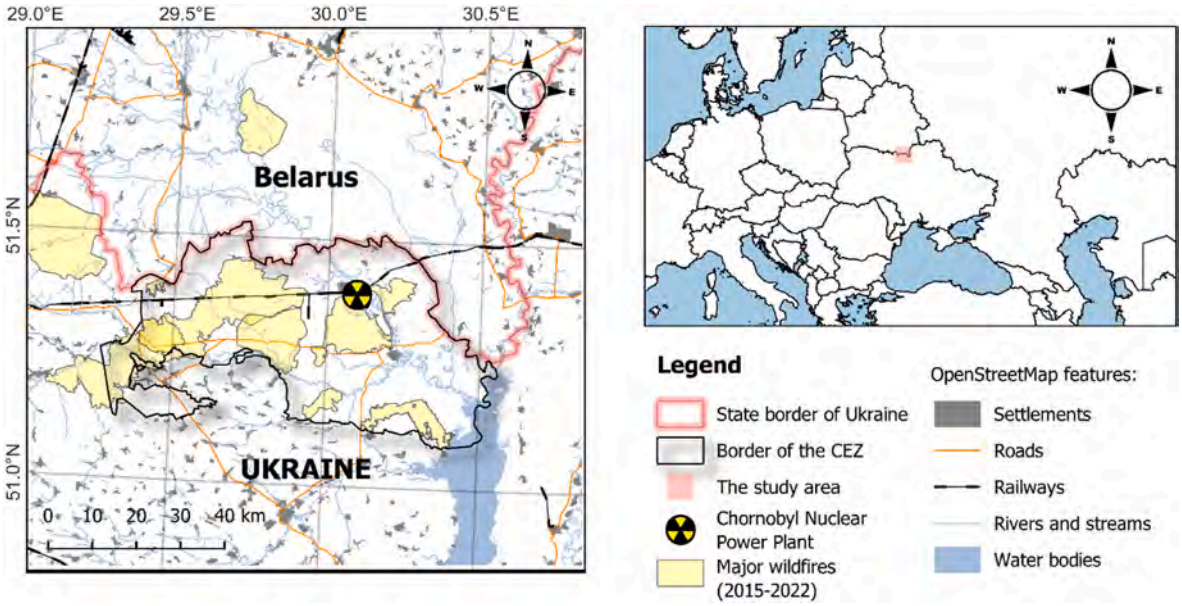

Fig. 1. The study area showing the locations of major wildfires that occurred in 2015–2022 within the CEZ and the surrounding areas.

sensor in our analysis. Clouds, cloud shadows, and snow were masked using pixel quality attributes generated from the CFMask algorithm (Foga et al., 2017) and available from the Pixel Quality Assessment band (QA_PIXEL). The Google Earth Engine (GEE) implementation of the CCDC segmentation algorithm (Zhu and Woodcock, 2014) was utilized to create temporally smoothed LTS. This approach is based on a harmonic regression to account for inter- and intra-annual cyclic patterns of spectral reflectance in line with the vegetation phenology over the year. The CCDC fits piecewise regression models between breakpoints that correspond to an abrupt surface change identified in available spectral bands. The segmentation is performed using time series of all clear observations, so there is no need to create image composites (e.g., monthly, seasonal, annual). The temporal segmentation of the LTS was performed using six original Landsat spectral bands that were combined with the Tasseled-Cap Transformation (TCT) brightness, greenness, and wetness (Crist and Cicone, 1984) as well as the Normalized Burn Ratio (NBR) (Key and Benson, 2006). The CCDC algorithm was applied using the default settings regarding probability thresholds to change detection, a minimal number of observations to flag changes, etc. (Zhu and Woodcock, 2014). As a result, we created an array image that stored sequences of temporal segments between detected breakpoints at 30-m spatial resolution. The coefficients of harmonic functions modeled within the segments can be used to generate smoothed (synthetic) imagery for any date within the specified timeframe.

2.2.2. *Reference data for land cover and fuel type classification*

A total of 1000 Landsat 30-m pixels randomly selected within the study area were used as a reference for the classification of land cover. Since our mapping approach aimed to classify the entire temporal segment rather than spectral data at a given time, the time series of high-resolution images available on Google Earth Pro were visually inspected to assign the corresponding land cover class. We analyzed the most recent images to identify a timeframe within which the pixel exhibited no land cover change. Depending on the availability of historical imagery, the reference data were interpreted between 2012 and 2022 to ensure the correct land cover class assignment. To determine the values for explanatory variables, the reference pixels were intersected with the corresponding temporal segments of the CCDC image. We followed the recommendation of the FirEUrisk project to harmonize the fuel classification scheme with existing ones in the European Union (Aragoneses and Chuvieco, 2021). Within this scheme, each fuel type (Scott and Burgan, 2005) is associated with the corresponding vegetation type influencing potential fire behavior (Table 1).

2.2.3. *GEDI canopy height metrics*

The GEDI is a system of three full waveform LiDAR sensors specially optimized for measuring vegetation structure. It samples the Earth's surface between ±51.6° N/S latitudes to generate data sets of vegetation properties and aboveground biomass (Dubayah et al., 2020). GEDI data are provided in different products representing different processing levels. Raw GEDI waveforms are processed to obtain ground elevation and relative height (RH) metrics for each 25-m footprint in the GEDI L2A Geolocated Elevation and Height Metrics (Version 2) product. The Level 2B Canopy Cover and Vertical Profile Metrics (Version 2) product include various canopy and vertical profile metrics extracted from each GEDI waveform. These two GEDI products that are available as public assets on GEE were utilized in our study. The L2A product (Healey et al., 2020) was used as reference data to characterize the vertical structure of forest stands using RH metrics. We extracted RH metrics for every five

Table 1
Distribution of sample size among land cover categories and associated fuel.

Land cover category	Land cover sub-category	Fuel model	Sample size in 30-m pixels
Forest	Coniferous	TL8	309
	Deciduous	TL2	105
	Mixed	TU1	49
	Burned forest	TL1	25
Grassland	Short grass (0–0.5 m)	GR1	69
	Medium grass (0.5–1.5 m)	GR2	104
	Grassland with shrubs	GS1	99
Cropland[a]	Fallow land (cropland)	GR1 (NB3)	136
Wetland	Peat, riparian vegetation	SH2	60
Water	Open water	NB8	17
Urban area and other unproductive lands	Infrastructure, sand	NB9	27

[a] Croplands exhibit a seasonal pattern of flammability, thus were classified as burnable fuel types in March–April and August–September (GR1) and unburnable fuels during May–July and October–February (NB3).

percentiles of energy return between RH10 and RH100 along with RH98. These metrics represent percentiles of energy return height relative to the ground return. Canopy cover (CC) was obtained from GEDI L2B variable list. Both variables were retrieved from GEE as rasterized mosaics (at 25-m spatial resolution) of the corresponding original GEDI products.

We used GEDI data collected throughout June–August of 2019–2022 to avoid issues with mixed phenology conditions (leaf-on and leaf-off). A total of ~736,000 observations ranged within the study area for the filtered time frame. We selected observations from power beams with beam sensitivity of more than 0.95 that had valid waveforms (quality_flag = 1) without positioning errors (degrade_flag = 0). These observations were resampled to Landsat 30-m spatial resolution to align footprints and pixel centers. Footprints located outside the forested areas were masked. Consequently, about 266,000 high-quality footprints were registered within our study area in power beams (Fig. 2a). A random subset of 2000 observations was used to predict CC and CH (Fig. 2b). Finally, we crossed acquisition dates of GEDI footprints with corresponding temporal segments of the CCDC image to extract coefficients and derivations (e.g., phase and amplitude) of the harmonic regression models.

2.3. Mapping approach

The RF classifier was used to produce a land cover map. Fuel types were mapped based on association between the land cover categories and the corresponding fuel models (Table 1). We tested various combinations of spectral variables and finally used three components of the TCT (brightness, greenness, wetness), NBR, red, near-infrared (NIR), and short-wave infrared (SWIR1) bands of the Landsat imagery. For each spectral band, we used an intercept, slope, and three sets of harmonic sin/cosine pairs that were combined with several derivations of the harmonic regression model, including phase, amplitude, and root mean square error (RMSE). We also calculated a density of observation for each segment and added this variable as a predictor in our RF model. The RF model was trained using a multi-date interpretation (between 2012 and 2020) of the reference data set linked to the 106 explanatory variables of the CCDC segments image.

We selected the RH95 metric as a measure of a stand's CH. For prediction, we used the gradient nearest neighbor (GNN) technique (Ohmann and Gregory, 2002) which is a multivariate modeling approach. One of important feature of the GNN imputation is that it can simultaneously predict a set of RH metrics and CC that characterize a plant community structure as a cohesive unit. Instead of modeling single response variables (e.g., RH95, CC), the GNN technique collectively predicts their realistic combinations (Henderson et al., 2014). The GEE implementation of the GNN algorithm (Myroniuk et al., 2022) was used to accelerate the imputation. For the GNN model, we used both CC and RH metrics as response variables and the list of CCDC covariates (which were employed in our RF model) as explanatory variables. Following Bell et al. (2015), we ascribed weights to the first seven nearest neighbors. The prediction of canopy metrics was calculated as the weighted mean of these neighbors.

2.4. Accuracy assessment

The map accuracy of fuel types was assessed using a leave-one-out cross-validation approach. We trained the RF model on all data except one observation retained for accuracy assessment. This procedure was repeated for each of 1000 samples. Then, we built an error matrix to estimate producer's (PA), user's (UA), and overall (OA) accuracies. We used a modified version of the leave-one-out procedure to assess the accuracy of the GNN model. This procedure utilized the pixel's first independent nearest neighbor (Ohmann and Gregory, 2002). Since we used the GNN model with $k = 7$, the first seven independent nearest neighbors were utilized in this study. The accuracy of the GNN model was assessed for the CC and the selected RH metrics. We used R-squared (R^2) and normalized root mean square error (NRMSE) values as the accuracy indicators of our model. They were estimated using observed and predicted mean values of the corresponding canopy metrics. We also built 1:1 identity plots to show the correspondence between observed and predicted values. The recommendations of Riemann et al. (2010) were also used to compare this with the geometric mean functional relationship (GMFR) which reflects both systematic (between the GFMR fit and 1:1 line) and unsystematic agreement (variance of GMFR fit) in the data.

3. Results

3.1. Spatiotemporal pattern of fuel type distribution

The CCDC classification allowed us to track a seasonal distribution of

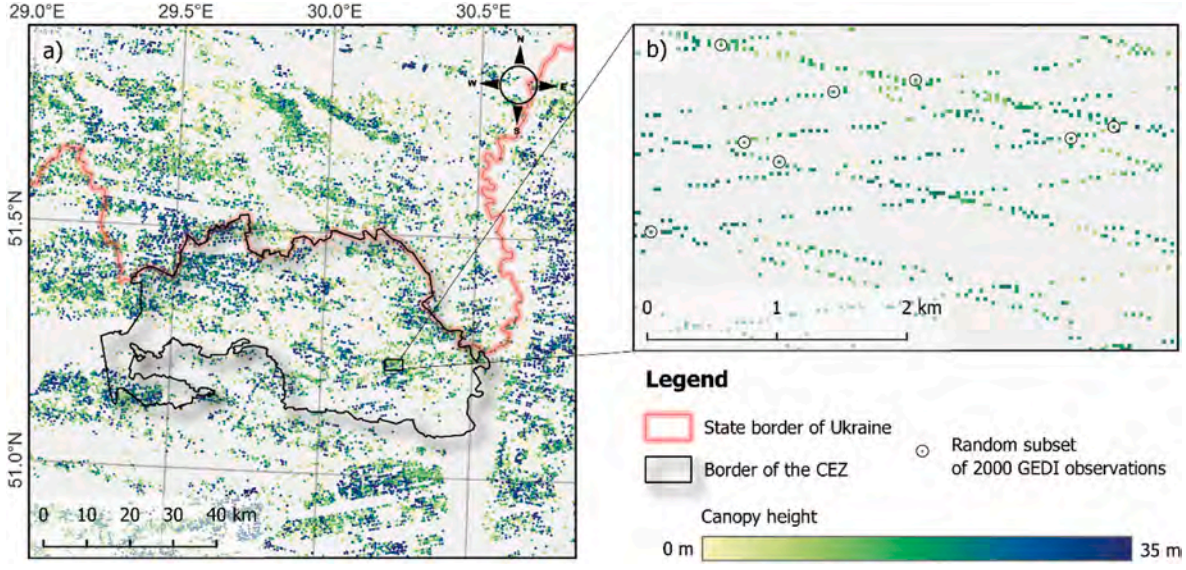

Fig. 2. Spatial distribution of the high-quality GEDI data from power beams within the forested areas: a) distribution of 25-m footprints; b) randomly sampled observations.

the flammable landscapes within the study area (Fig. 3). Fuel type maps generated for different seasons showed spatial variation in the distribution of burnable landscapes mostly outside the CEZ. We detected croplands that cause early spring and fall grass fires on the edge of the CEZ. However, the intra-annual change between burnable (GR1) and non-burnable (NB3) fuel types typical for croplands introduces seasonality for transmitting fire into the CEZ.

The overall accuracy of the RF model at 30-m spatial resolution (Landsat pixel level) was 0.75. The CCDC-classification approach demonstrated high user's and producer's accuracies in mapping non-burnable (NB8 and NB9) surfaces (Table 2). Accuracy values above 0.7 were observed for all three TL fuel types (i.e., TL1, TL2, and TL8), showing good performance in the classification method applied. However, CCDC classification for mixed forests (TU1) resulted in lower accuracies as observed in the computed commission and emission errors (UA = 0.48, PA = 0.24). Expectedly, we identified that this fuel type was mostly misclassified between another two forested vegetation types (TL1 and TL8) that occupied a much larger area. We obtained medium (about 0.6–0.8) user's accuracies for non-forested vegetation (i.e., GR, GS, and SH fuel types); however, the producer's accuracies here varied from poor (0.4) to better (0.6–0.7). Importantly, the CCDC-based classification of temporal trajectories allowed mapping croplands (NB3) with good accuracy (both UA and PA were greater than 0.8).

3.2. Mapping canopy metrics

The GNN model with $k = 7$ at 30-m spatial resolution attained a higher accuracy to predict relative height metrics RH70 and RH80 for which *R*-squared reached value of 0.27 (Table 3). The RH95 used in this study as a proxy for average stand height was estimated with slightly lower *R*-squared value ($R^2 = 0.23$). We also observed an overestimation of the mean imputed values of all relative height metrics (estimated using seven independent nearest neighbors) compared to the corresponding observed means of our training data set (2000 random samples). Based on the same seven nearest neighbors, the GNN model demonstrated similar predictive performance for the canopy cover ($R^2 = 0.26$; NRMSE = 0.37) and an exact correspondence between observed and predicted mean values of canopy cover (0.5).

Scatterplots of observed and predicted values of CH (RH95) and CC at 30-m pixel level showed fair agreement with the 1:1 identity line (Fig. 4a and b). Insignificant overestimations of the mean values of the CH and CC (see Table 3) occurred due to the weak performance of the GNN model for low values (a dashed line of GMFR fit was above the solid 1:1 identity line). In general, we observed a significant scattering of the data which is characterized by relatively low *R*-squared values (0.23–0.26) and high NRMSE (0.32–0.37). However, we identified a fair systematic agreement between the observed and predicted values.

3.3. Fuel type dynamics

During the period of 2012–2022, the CEZ experienced a significant land cover transformation that caused a change in fuel type distribution over the territory (Fig. 5). The wildfires of 2015, 2020, and 2022 made a major contribution to the transition between forested and non-forested

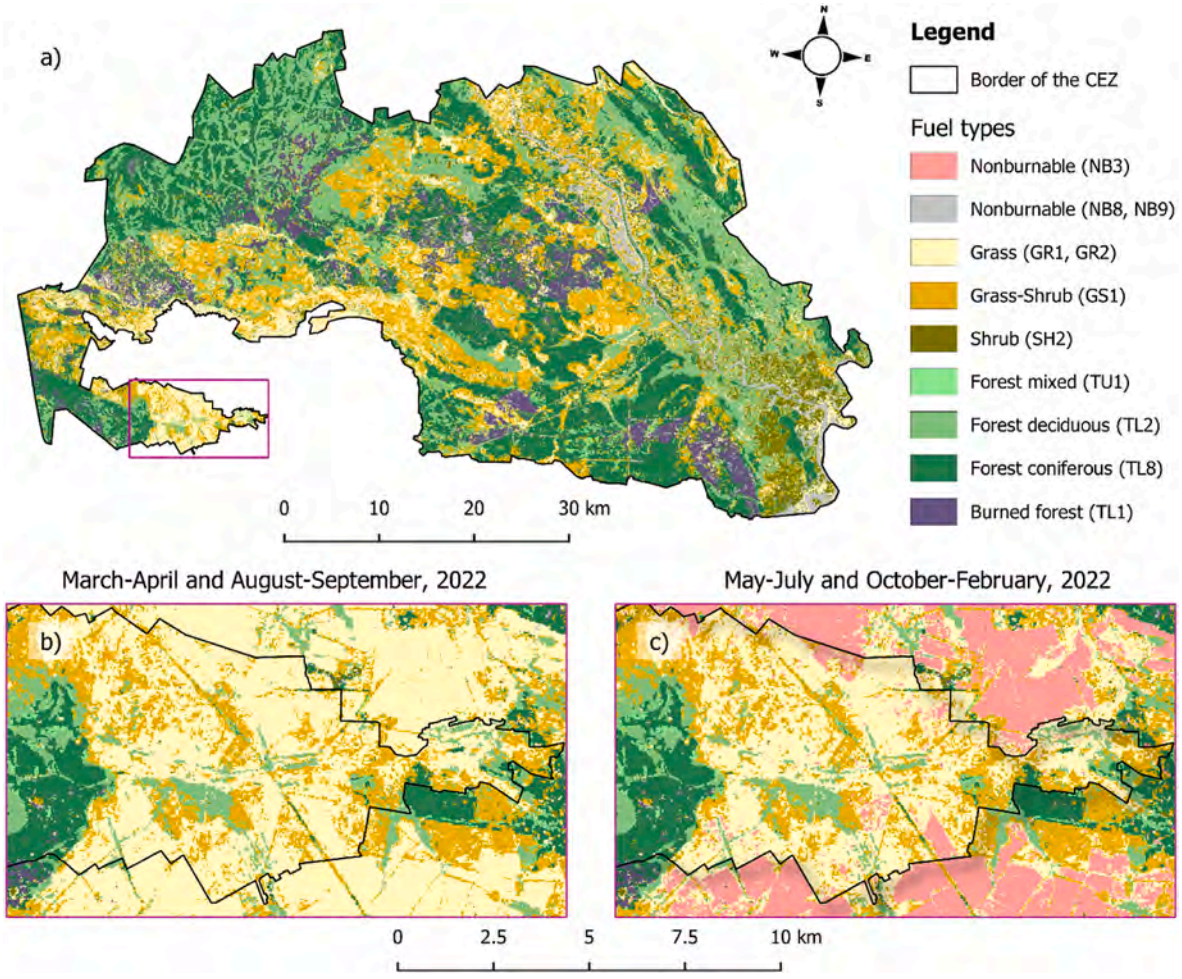

Fig. 3. CCDC-based classification of fuel types within the CEZ for 2022 (a). Croplands can be classified as burnable herbaceous fuel types during the early spring and fall seasons (b) or as areas kept in non-burnable condition during a growing phase and overwintering (c).

Table 2
LOOCV confusion matrix of fuel type mapping based on the CCDC approach.

Mapped fuel model	Reference fuel model											Total	UA	PA
	NB3	NB8	NB9	GR1	GR2	GS1	SH2	TU1	TL1	TL2	TL8			
NB3	120		3	9	7	2	4		2			147	0.82	0.88
NB8		17	1									18	0.94	1.00
NB9	1		19	3					3			26	0.73	0.70
GR1	7			28	2	5						42	0.67	0.41
GR2	7			7	73	9	22	1		4	1	124	0.59	0.70
GS1	1		2	18	11	63	2	4		5	5	111	0.57	0.64
SH2					2		23			3		28	0.82	0.38
TU1					2	1		12		2	8	25	0.48	0.24
TL1			1						19			20	0.95	0.76
TL2				1	7	9	6	11		84	1	119	0.71	0.80
TL8			1	3		10	3	21	1	7	294	340	0.86	0.95
Total	136	17	27	69	104	99	60	49	25	105	309	1000	–	–

NB3 – fallow land (cropland); NB8 – open water; NB9 – infrastructure, sand; GR1 – short grass; GR2 – medium grass; GS1 – grassland with trees; SH2 – peat, riparian vegetation; TU1 – mixed forest; TL1 – burned forest; TL2 – deciduous forest; TL8 – coniferous forest.

Table 3
Prediction accuracy of the GNN model ($k = 7$) by canopy metrics.

Canopy relative height	Mean, m		Normalized RMSE	R^2
	Observed	Predicted		
RH50	9.6	9.9	0.64	0.23
RH60	11.9	12.3	0.53	0.26
RH70	13.9	14.3	0.46	0.27
RH80	15.8	16.1	0.40	0.27
RH90	18.0	18.3	0.35	0.25
RH95	19.4	19.7	0.32	0.23
RH98	20.6	21.0	0.31	0.20

landscapes. The fuel type map derived using the CCDC approach for 2022 shows a large area of burned forests both within and outside the CEZ. Another interesting feature of the landscape was a drained CNPP cooling pond, which contributed in 2022 to the increase of territories with the dominance of herbaceous fuels.

Wildfires made a major impact on the distribution of fuel types within the CEZ (Fig. 6). We observed an increase in the area of burned forests (TL1) and vegetation dominated by shrubs and grasses (GS1; GR1, GR2) that replaced predominantly coniferous forest (TL8). The dynamics of the rest of fuel types were not so obvious during the reported period. However, the wildfires also affected forested areas outside the CEZ (see Fig. 5).

During the last decade, we observed a significant change in CC within the footprints of large fires (Fig. 7). The comparison of imputed maps of 2012 and 2022 also revealed a reduction of CH within these burned areas. Over other areas any remarkable trends in CC and CH change have not been identified.

4. Discussion

4.1. Delivering intra-annual and inter-annual variation of fuel pattern to wildfire risk assessment

The CCDC classification demonstrated high accuracy in cropland mapping, improving our understanding of the seasonal variability of wildfire risks. Using temporal segmentation algorithms, we classified croplands with accuracies of 0.82–0.88, indicating the importance of intra-annual variations of spectral information in classification models. The advantage of temporal segmentation algorithms in capturing seasonal trends of vegetation has been reported by Mardian et al. (2021) who achieved similar detection accuracy in grasslands to croplands conversion using remote sensing time series.

Our mapping approach revealed that the spatial pattern of burnable and non-burnable fuel types changes significantly throughout the year (Fig. 3). It was also able to adequately separate arable lands from other types of natural grassy vegetation. During the vegetation growth cycle, the croplands located outside of the CEZ were classified as GR1 when farmers can burn dried vegetation residuals (March–April and September–August). At other times (May–July), such areas were characterized with the NB3 model. The CCDC mapping approach provides a sound basis for such work as it allows land cover and associated fuel type maps to be obtained for any date within the available time series of satellite imagery.

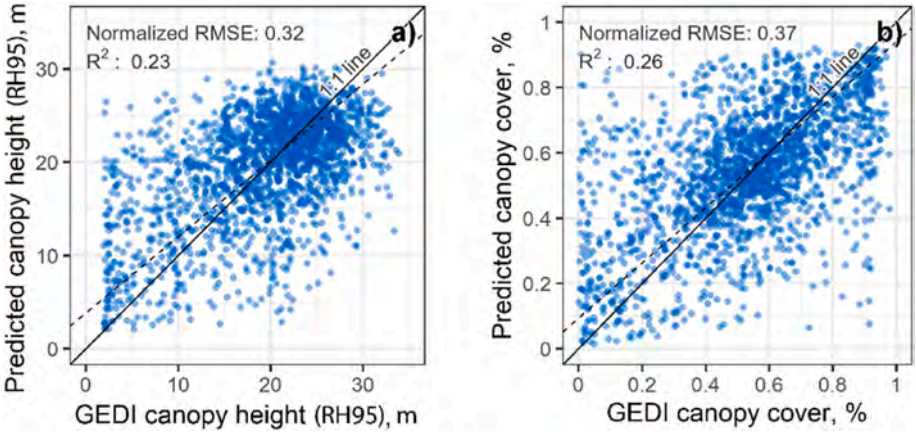

Fig. 4. Predicted versus observed values of the GEDI canopy metrics. A dashed line shows the GMFR fit line describing the relationship between the predicted and observed data.

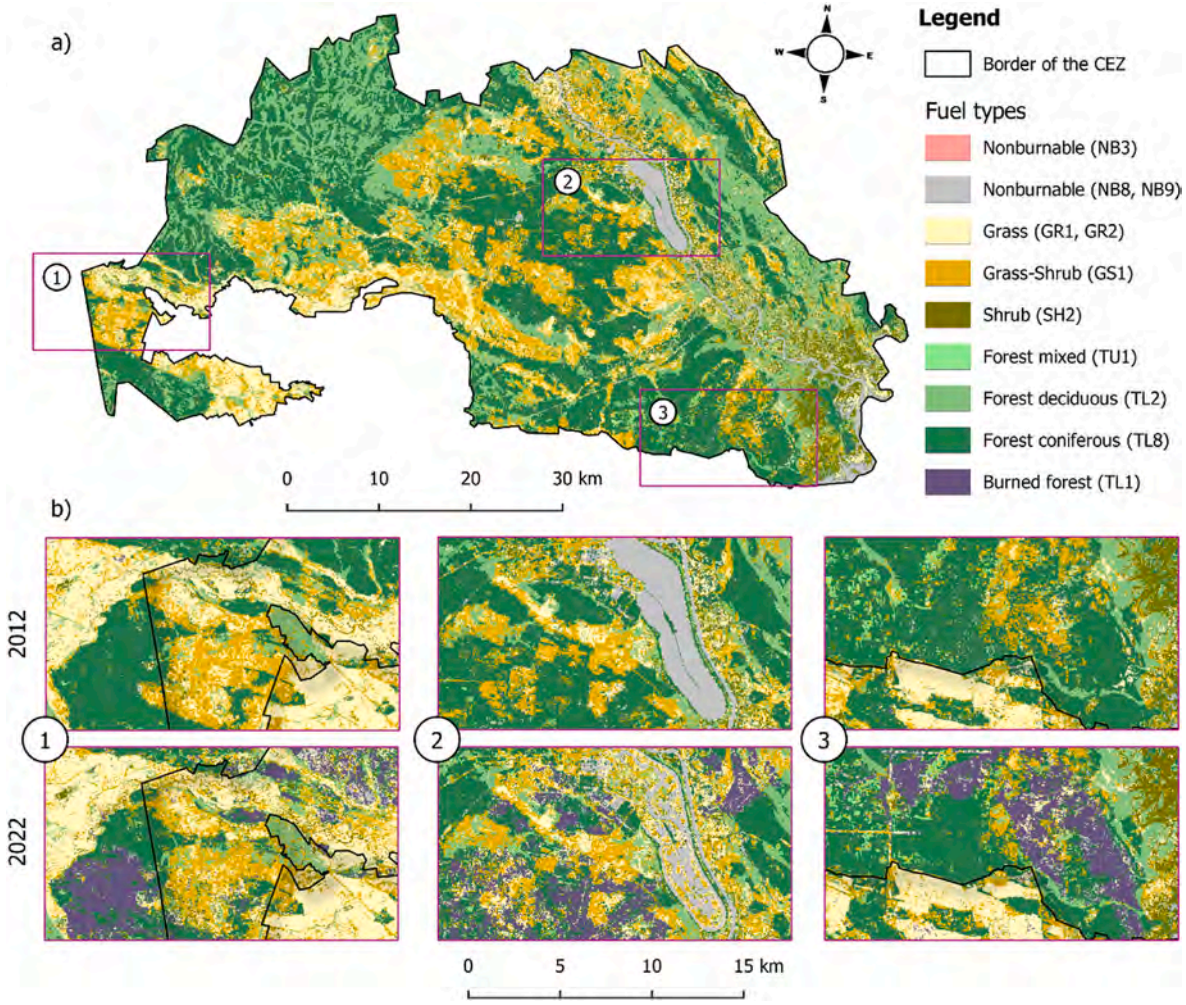

Fig. 5. Fuel type dynamics within the study area between 2012 and 2022: a) fuel type map for 2012; b) close-up examples showing fuel type transitions in sampled areas (1–3) within and outside the CEZ.

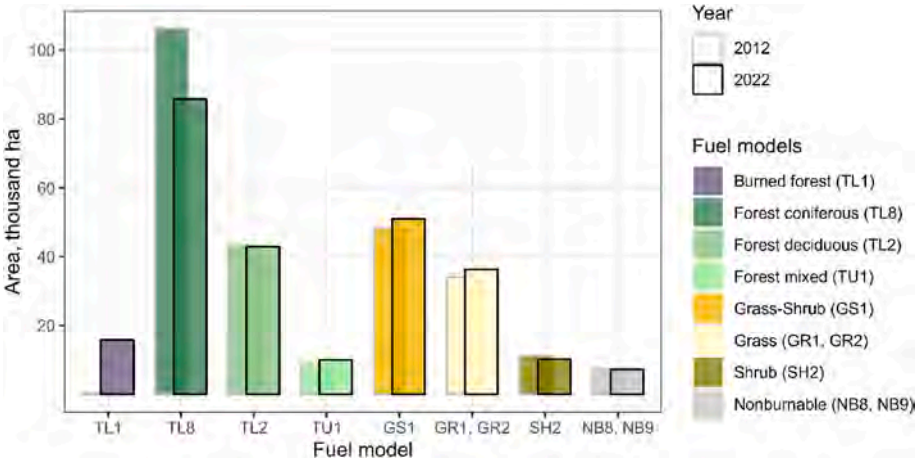

Fig. 6. Dynamics of fuel types within the boundaries of the CEZ (area estimates are not reported for the entire study area as this is rather synthetic).

4.2. The role of GEDI data and LTS in canopy fuels characterization

This study demonstrated the potential of the nearest neighbor imputation technique to extrapolate GEDI observations for a spatially explicit characterization of CC and CH using optical data. Similarly to other studies (e.g., Wilson et al., 2018), we found that temporal metrics extracted from time series of satellite data are more useful for mapping key forest attributes than merely spectral observations. The GNN model has also shown promising results for simultaneous prediction of various RH metrics. The GNN imputation technique to treat footprint-level data as characteristics of a stacked vegetation community unit (Ohmann et al., 2011) can be used to extrapolate realistic combinations of RH

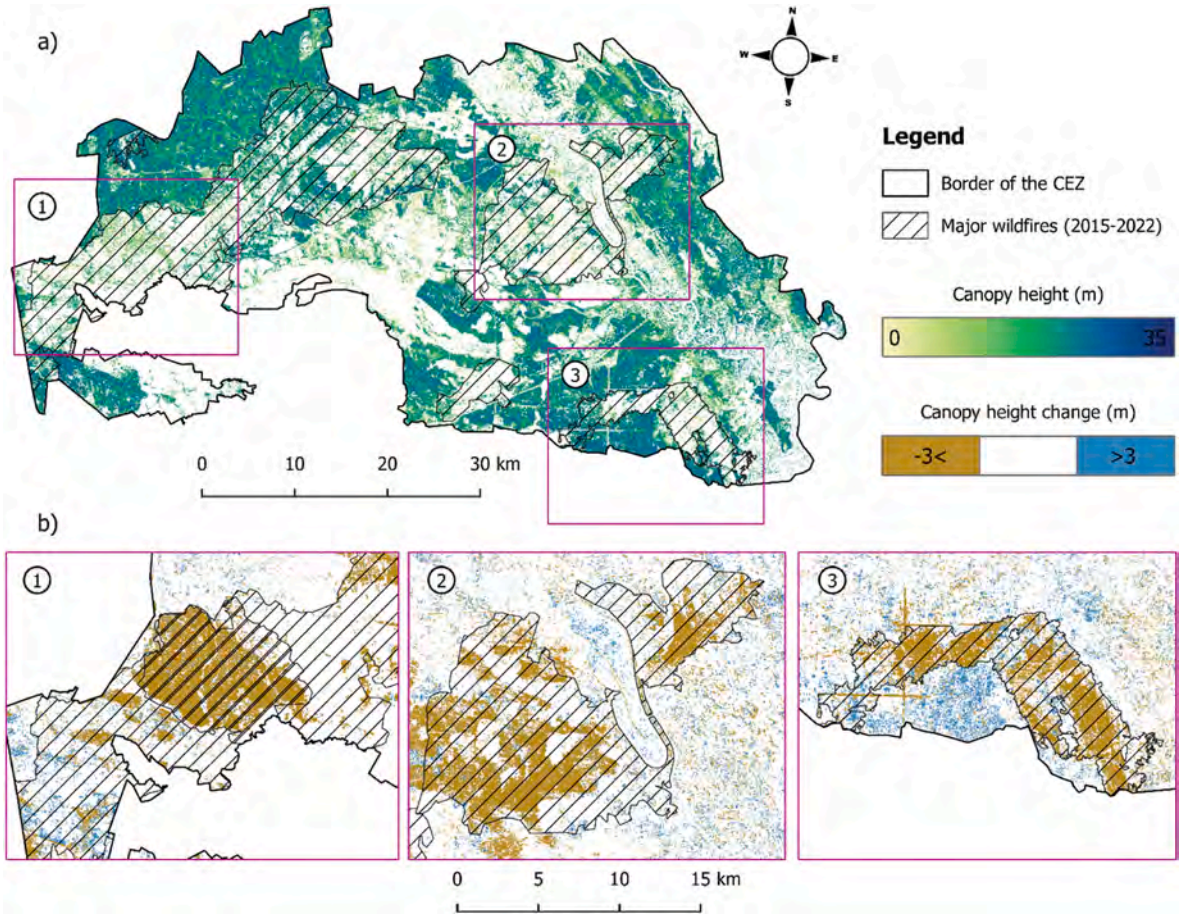

Fig. 7. Predicted canopy height for 2022 (a) and its decadal dynamic (b) in sampled areas (1–3).

metrics observed at GEDI footprints. This provides the basis for mapping canopy base height (CBH) which is another important characteristic of canopy fuels used in wildfire simulation.

The performance of the GNN imputation model was lower than in other published studies. For example, Potapov et al. (2021) modeled canopy height (RH95) combining GEDI observations with LTS and achieved R^2 values of 0.61–0.62. However, issues relevant to characterizing the vertical structure of forest ecosystems using optical satellite data were reported by Matasci et al. (2018). Despite good performance of a nearest imputation technique in terms of predicting aboveground biomass and other variables that correlates better with LTS indices, obtained R^2 values did not exceed 0.61 for variables related to stand height. Thus, GEDI data demonstrated superior accuracy in predicting canopy heights using the full LiDAR waveforms and deep learning algorithms (Fayad et al., 2021). Relatively low values of R^2 in our study for height metrics modeling can be also explained by the character of the data distribution used in this study. Specifically, we excluded zero values from our data set within unforested areas to avoid inflating R^2 values where our method is not applicable. Bolton et al. (2020) demonstrated that short LTS length can also resul in weak model accuracy, as measured by R^2.

4.3. Limitations and potential improvements for large-scale applications

The use of CCDC-fitted LTS for land cover mapping has been extensively investigated in the literature (Pasquarella et al., 2022). While broad land cover categories can be directly identified using visual photointerpretation of high-resolution imagery, the correct interpretation of fuel types is not straightforward. However, fuels that belong to the same fire-carrying fuel type (Scott and Burgan, 2005) can exhibit very different fire spread potential. For example, misinterpretation of grassy vegetations fuels (e.g., GR1 and GR2) can cause confusion between mapped classes (Table 2) and thus potentially affecting the fire simulation results. Apart from this obstacle, we found the CCDC approach to be very effective for updated mapping of fuel continuity once new Landsat data are available. Further development of this approach is possible due to the long time series of Sentinel 2 images that have been collected globally since 2015.

Previous studies combining fuel characteristics at sample plots and GEDI data showed their usefulness in establishing frameworks for fire management (Hoffrén et al., 2023). By providing detailed structural information, the GEDI instrument facilitates the assessment of fuel loads at large geographical scales. The most significant limitation of our study is the lack of field measurements coupled with GEDI full waveforms to calibrate fuel loading models at test sites (Leite et al., 2022). Therefore, we focused on canopy metrics available in GEDI products. Integration of footprint-level LiDAR observations with LTS can support wall-to-wall mapping using accurate modeling and reliable reference data (Wang et al., 2022). The GNN imputation technique has shown promise for simultaneous prediction of a set of canopy metrics using LTS. However, the limitations of the proposed approach to extrapolate GEDI data can relate to the Landsat signal saturation that occurs for stands with closed canopy or dense understory (Healey et al., 2020). In our study, this was supported by relatively low R^2 values (0.20–0.26).

Application of synthetic aperture radar (SAR) data could be an option to reliably extrapolate the estimates of stand vertical structure. SAR sensors with long wavelengths (e.g., operating ALOS-PALSAR 2 with 22.9 cm L-band or future BIOMASS mission with 69 cm P-band) can be used to overcome biomass saturation issues as they are more sensitive to important tree structures like trunks and large branches (Ngo et al.,

2022). Additionally, polarimetric tomography methods are able to provide direct wall-to-wall canopy height estimates for a given scene (Ho Tong Minh et al., 2016). Nevertheless, the results we obtained look promising for large-scale characterization of canopy fuels in wildfire simulation studies which can rely on higher aggregation levels (e.g., 3 × 3 pixels) and be more relevant than footprint-level accuracy (Riemann et al., 2010).

5. Conclusion

This study demonstrates an approach to systematically updating fuel type maps and some canopy metrics needed to model wildfire in radioactively contaminated areas where field data collection is challenging. The introduction of temporal trajectories of spectral features extracted from LTS was able to attain an adequate overall accuracy (OA = 75%) in mapping land covers and associated fuel types. The proposed approach to fuel type mapping demonstrated two main advantages. First, the fitted CCDC harmonic regression models can effectively track intra-annual changes in spectral dynamics that are specific to a certain land cover. We showed that these trends can be used to more accurate classify similar types of vegetation (e.g., grasslands and croplands) that exhibit different flammability throughout the year. Second, the time series classification ensured a logical sequence of the mapped land cover classes at 30-m pixel unless abrupt changes were observed. GEDI data combined with LTS showed a promising utility in the generation of CH and CC used in wildfire simulation. What differentiates our approach is that all these layers can be simultaneously extracted for a given date and canopy metrics can be obtained using the spatial coverage of forested areas from the fuel type layer. We also hypothesize that GEDI data can contribute to a spatially explicit representation of other important canopy fuels data (i.e., CBH and CBD). However, additional work is needed to incorporate them into our workflow.

Credit authors statement

Viktor Myroniuk: Conceptualization, Methodology, Data curation, Formal analysis, Software, Validation, Visualization, Writing – original draft, Writing – review & editing. Sergiy Zibtsev: Funding acquisition, Writing – original draft, Writing – review & editing. Vadym Bogomolov: Data curation, Formal analysis. Johann Georg Goldammer: Funding acquisition, Writing – original draft. Oleksandr Soshenskyi: Data curation, Investigation. Viacheslav Levchenko: Validation. Maksym Matsala: Methodology, Writing – original draft, Writing – review & editing.

Funding

The research in CEZ funded by European Union's Horizon 2020 Program within the project FirEUrisk "Development a holistic, risk-wise strategy for European wildfire management" (Grant agreement ID 101003890) and Ministry of Education and Science of Ukraine (Grants No. 0121U109960; 0121U110106).

Declaration of competing interest

The authors declare that they have no known competing financial interests or personal relationships that could have appeared to influence the work reported in this paper.

Data availability

Data will be made available on request.

Acknowledgement

The authors are grateful to Matthew J. Gregory for providing an access to the GEE-implemented library (GEE-KNN) which automated the GNN imputation. The authors are also thankful to two anonymous reviewers for their very helpful and constructive comments.

References

Ager, A.A., Lasko, R., Myroniuk, V., Zibtsev, S., Day, M.A., Usenia, U., Bogomolov, V., Kovalets, I., Evers, C.R., 2019. The wildfire problem in areas contaminated by the Chernobyl disaster. Sci. Total Environ. 696, 133954 https://doi.org/10.1016/j.scitotenv.2019.133954.

Alcasena, F., Salis, M., Ager, A., Castell, R., Vega-García, C., 2017. Assessing wildland fire risk transmission to communities in Northern Spain. Forests 8 (2), 30. https://doi.org/10.3390/f8020030.

Andersen, H.-E., McGaughey, R.J., Reutebuch, S.E., 2005. Estimating forest canopy fuel parameters using LIDAR data. Remote Sens. Environ. 94 (4), 441–449. https://doi.org/10.1016/j.rse.2004.10.013.

Aragoneses, E., Chuvieco, E., 2021. Generation and mapping of fuel types for fire risk assessment. Fire 4 (3), 59. https://doi.org/10.3390/fire4030059.

Bell, D.M., Gregory, M.J., Ohmann, J.L., 2015. Imputed forest structure uncertainty varies across elevational and longitudinal gradients in the western Cascade Mountains, Oregon, USA. For. Ecol. Manag. 358, 154–164. https://doi.org/10.1016/j.foreco.2015.09.007.

Bolton, D.K., Tompalski, P., Coops, N.C., White, J.C., Wulder, M.A., Hermosilla, T., Queinnec, M., Luther, J.E., van Lier, O.R., Fournier, R.A., Woods, M., Treitz, P.M., van Ewijk, K.Y., Graham, G., Quist, L., 2020. Optimizing Landsat time series length for regional mapping of lidar-derived forest structure. Remote Sens. Environ. 239, 111645 https://doi.org/10.1016/j.rse.2020.111645.

Chuvieco, E., Aguado, I., Salas, J., García, M., Yebra, M., Oliva, P., 2020. Satellite remote sensing contributions to wildland fire science and management. Current Forestry Reports 6 (2), 81–96. https://doi.org/10.1007/s40725-020-00116-5.

Crist, E.P., Cicone, R.C., 1984. Comparisons of the dimensionality and features of simulated Landsat-4 MSS and TM data. Remote Sens. Environ. 14 (1–3), 235–246. https://doi.org/10.1016/0034-4257(84)90018-X.

Dorado-Roda, I., Pascual, A., Godinho, S., Silva, C., Botequim, B., Rodríguez-Gonzálvez, P., González-Ferreiro, E., Guerra-Hernández, J., 2021. Assessing the accuracy of GEDI data for canopy height and aboveground biomass estimates in Mediterranean forests. Rem. Sens. 13 (12), 2279. https://doi.org/10.3390/rs13122279.

Dubayah, R., Armston, J., Healey, S.P., Bruening, J.M., Patterson, P.L., Kellner, J.R., Duncanson, L., Saarela, S., Ståhl, G., Yang, Z., Tang, H., Blair, J.B., Fatoyinbo, L., Goetz, S., Hancock, S., Hansen, M., Hofton, M., Hurtt, G., Luthcke, S., 2022. GEDI launches a new era of biomass inference from space. Environ. Res. Lett. 17 (9), 095001 https://doi.org/10.1088/1748-9326/ac8694.

Dubayah, R., Blair, J.B., Goetz, S., Fatoyinbo, L., Hansen, M., Healey, S., Hofton, M., Hurtt, G., Kellner, J., Luthcke, S., Armston, J., Tang, H., Duncanson, L., Hancock, S., Jantz, P., Marselis, S., Patterson, P.L., Qi, W., Silva, C., 2020. The global ecosystem dynamics investigation: high-resolution laser ranging of the Earth's forests and topography. Science of Remote Sensing 1, 100002. https://doi.org/10.1016/j.srs.2020.100002.

Dwiputra, A., Coops, N.C., Schwartz, N.B., 2023. GEDI waveform metrics in vegetation mapping—a case study from a heterogeneous tropical forest landscape. Environ. Res. Lett. 18 (1), 015007 https://doi.org/10.1088/1748-9326/acad8d.

Evangeliou, N., Zibtsev, S., Myroniuk, V., Zhurba, M., Hamburger, T., Stohl, A., Balkanski, Y., Paugam, R., Mousseau, T.A., Møller, A.P., Kireev, S.I., 2016. Resuspension and atmospheric transport of radionuclides due to wildfires near the Chernobyl Nuclear Power Plant in 2015: an impact assessment. Sci. Rep. 6 https://doi.org/10.1038/srep26062.

Fayad, I., Ienco, D., Baghdadi, N., Gaetano, R., Alvares, C.A., Stape, J.L., Ferraço Scolforo, H., Le Maire, G., 2021. A CNN-based approach for the estimation of canopy heights and wood volume from GEDI waveforms. Remote Sens. Environ. 265, 112652 https://doi.org/10.1016/j.rse.2021.112652.

Fedoniuk, T., Borsuk, O., Melnychuk, T., Zymaroieva, A., Pazych, V., 2021. Assessment of the consequences of forest fires in 2020 on the territory of the Chornobyl radiation and ecological biosphere reserve. Scientific Horizons 24 (8), 26–36. https://doi.org/10.48077/scihor.24(8).2021.26-36.

Foga, S., Scaramuzza, P.L., Guo, S., Zhu, Z., Dilley, R.D., Beckmann, T., Schmidt, G.L., Dwyer, J.L., Joseph Hughes, M., Laue, B., 2017. Cloud detection algorithm comparison and validation for operational Landsat data products. Remote Sens. Environ. 194, 379–390. https://doi.org/10.1016/j.rse.2017.03.026.

Francini, S., D'Amico, G., Vangi, E., Borghi, C., Chirici, G., 2022. Integrating GEDI and landsat: spaceborne lidar and four decades of optical imagery for the analysis of forest disturbances and biomass changes in Italy. Sensors 22 (5). https://doi.org/10.3390/s22052015, 2015.

Healey, S.P., Yang, Z., Gorelick, N., Ilyushchenko, S., 2020. Highly local model calibration with a new GEDI LiDAR asset on Google earth engine reduces landsat forest height signal saturation. Rem. Sens. 12 (17), 2840. https://doi.org/10.3390/rs12172840.

Henderson, E.B., Ohmann, J.L., Gregory, M.J., Roberts, H.M., Zald, H., 2014. Species distribution modelling for plant communities: stacked single species or multivariate modelling approaches? Appl. Veg. Sci. 17 (3), 516–527. https://doi.org/10.1111/avsc.12085.

Ho Tong Minh, D., Le Toan, T., Rocca, F., Tebaldini, S., Villard, L., Réjou-Méchain, M., Phillips, O.L., Feldpausch, T.R., Dubois-Fernandez, P., Scipal, K., Chave, J., 2016. SAR tomography for the retrieval of forest biomass and height: cross-validation at two tropical forest sites in French Guiana. Remote Sens. Environ. 175, 138–147. https://doi.org/10.1016/j.rse.2015.12.037.

Hoffrén, R., Lamelas, M.T., de la Riva, J., Domingo, D., Montealegre, A.L., García-Martín, A., Revilla, S., 2023. Assessing GEDI-NASA system for forest fuels classification using machine learning techniques. Int. J. Appl. Earth Obs. Geoinf. 116, 103175 https://doi.org/10.1016/j.jag.2022.103175.

Kalabokidis, K., Ager, A., Finney, M., Athanasis, N., Palaiologou, P., Vasilakos, C., 2016. AEGIS: a wildfire prevention and management information system. Nat. Hazards Earth Syst. Sci. 16 (3), 643–661. https://doi.org/10.5194/nhess-16-643-2016.

Kashparov, V.A., Zhurba, M.A., Kireev, S.I., Zibtsev, S.V., Myroniuk, V.V., 2015. Evaluation of the expected doses of fire brigades at the Chornobyl exclusion Zone in April 2015. Nuclear Physics and Atomic Energy 16 (4), 399–407. https://doi.org/10.15407/jnpae2015.04.399.

Key, C.H., Benson, N.C., 2006. Landscape Assessment (LA): Sampling and Analysis Methods (General Technical Report RMRS-GTR-164; FIREMON: Fire Effects Monitoring and Inventory System, P. LA-1-LA-51). Rocky Mountain Research Station, US Department of Agriculture, Forest Service.

Leite, R.V., Silva, C.A., Broadbent, E.N., Amaral, C. H. do, Liesenberg, V., Almeida, D. R. A. de, Mohan, M., Godinho, S., Cardil, A., Hamamura, C., Faria, B. L. de, Brancalion, P.H.S., Hirsch, A., Marcatti, G.E., Dalla Corte, A.P., Zambrano, A.M.A., Costa, M. B. T. da, Matricardi, E.A.T., Silva, A. L. da, Klauberg, C., 2022. Large scale multi-layer fuel load characterization in tropical savanna using GEDI spaceborne lidar data. Remote Sens. Environ. 268, 112764 https://doi.org/10.1016/j.rse.2021.112764.

Maltamo, M., Räty, J., Korhonen, L., Kotivuori, E., Kukkonen, M., Peltola, H., Kangas, J., Packalen, P., 2020. Prediction of forest canopy fuel parameters in managed boreal forests using multispectral and unispectral airborne laser scanning data and aerial images. European Journal of Remote Sensing 53 (1), 245–257. https://doi.org/10.1080/22797254.2020.1816142.

Mardian, J., Berg, A., Daneshfar, B., 2021. Evaluating the temporal accuracy of grassland to cropland change detection using multitemporal image analysis. Remote Sens. Environ. 255, 112292 https://doi.org/10.1016/j.rse.2021.112292.

Matasci, G., Hermosilla, T., Wulder, M.A., White, J.C., Coops, N.C., Hobart, G.W., Bolton, D.K., Tompalski, P., Bater, C.W., 2018. Three decades of forest structural dynamics over Canada's forested ecosystems using Landsat time-series and lidar plots. Remote Sens. Environ. 216, 697–714. https://doi.org/10.1016/j.rse.2018.07.024.

Matsala, M., Bilous, A., Myroniuk, V., Diachuk, P., Burianchuk, M., Zadorozhniuk, R., 2021a. Natural forest regeneration in Chernobyl Exclusion Zone: predictive mapping and model diagnostics. Scand. J. For. Res. 1–13. https://doi.org/10.1080/02827581.2021.1890816.

Matsala, M., Bilous, A., Myroniuk, V., Holiaka, D., Schepaschenko, D., See, L., Kraxner, F., 2021b. The return of nature to the chernobyl exclusion Zone: increases in forest cover of 1.5 times since the 1986 disaster. Forests 12 (8), 1024. https://doi.org/10.3390/f12081024.

Moeur, M., Stage, A.R., 1995. Most similar neighbor—an improved sampling inference procedure for natural-resource planning. For. Sci. 41 (2), 337–359.

Moran, C.J., Kane, V.R., Seielstad, C.A., 2020. Mapping forest canopy fuels in the western United States with LiDAR–landsat covariance. Rem. Sens. 12 (6), 1000. https://doi.org/10.3390/rs12061000.

Mutlu, M., Popescu, S., Stripling, C., Spencer, T., 2008. Mapping surface fuel models using lidar and multispectral data fusion for fire behavior. Remote Sens. Environ. 112 (1), 274–285. https://doi.org/10.1016/j.rse.2007.05.005.

Myroniuk, V., Bell, D.M., Gregory, M.J., Vasylyshyn, R., Bilous, A., 2022. Uncovering forest dynamics using historical forest inventory data and Landsat time series. For. Ecol. Manag. 513, 120184 https://doi.org/10.1016/j.foreco.2022.120184.

Myroniuk, V., Zibtsev, S., Bogomolov, V., Soshenskyi, O., Gumeniuk, V., Vasylyshyn, R., 2021. A web-based platform LANDSCAPE FIRES: regional-level fire management information system for Northern Ukraine. Geoinformatics 1–6. https://doi.org/10.3997/2214-4609.20215521113.

Ngo, Y.-N., Huang, Y., Minh, D.H.T., Ferro-Famil, L., Fayad, I., Baghdadi, N., 2022. Tropical forest vertical structure characterization: from GEDI to P-band SAR tomography. Geosci. Rem. Sens. Lett. IEEE 19, 1–5. https://doi.org/10.1109/LGRS.2022.3208744.

Ohmann, J.L., Gregory, M.J., 2002. Predictive mapping of forest composition and structure with direct gradient analysis and nearest- neighbor imputation in coastal Oregon, U.S.A. Can. J. For. Res. 32 (4), 725–741. https://doi.org/10.1139/x02-011.

Ohmann, J.L., Gregory, M.J., Henderson, E.B., Roberts, H.M., 2011. Mapping gradients of community composition with nearest-neighbour imputation: Extending plot data for landscape analysis: Extending plot data for landscape analysis. J. Veg. Sci. 22 (4), 660–676. https://doi.org/10.1111/j.1654-1103.2010.01244.x.

Pasquarella, V.J., Arévalo, P., Bratley, K.H., Bullock, E.L., Gorelick, N., Yang, Z., Kennedy, R.E., 2022. Demystifying LandTrendr and CCDC temporal segmentation. Int. J. Appl. Earth Obs. Geoinf. 110, 102806 https://doi.org/10.1016/j.jag.2022.102806.

Potapov, P., Li, X., Hernandez-Serna, A., Tyukavina, A., Hansen, M.C., Kommareddy, A., Pickens, A., Turubanova, S., Tang, H., Silva, C.E., Armston, J., Dubayah, R., Blair, J. B., Hofton, M., 2021. Mapping global forest canopy height through integration of GEDI and Landsat data. Remote Sens. Environ. 253, 112165 https://doi.org/10.1016/j.rse.2020.112165.

Reeves, M.C., Ryan, K.C., Rollins, M.G., Thompson, T.G., 2009. Spatial fuel data products of the LANDFIRE Project. Int. J. Wildland Fire 18 (3), 250. https://doi.org/10.1071/WF08086.

Riemann, R., Wilson, B.T., Lister, A., Parks, S., 2010. An effective assessment protocol for continuous geospatial datasets of forest characteristics using USFS Forest Inventory and Analysis (FIA) data. Remote Sens. Environ. 114 (10), 2337–2352. https://doi.org/10.1016/j.rse.2010.05.010.

Rishmawi, K., Huang, C., Zhan, X., 2021a. Monitoring Key Forest Structure Attributes across the Conterminous United States by Integrating GEDI LiDAR Measurements and VIIRS Data. Rem. Sens. 13 (3), 442. https://doi.org/10.3390/rs13030442.

Rishmawi, K., Huang, C., Zhan, X., 2021b. Monitoring Key Forest Structure Attributes across the Conterminous United States by Integrating GEDI LiDAR Measurements and VIIRS Data. Rem. Sens. 13 (3), 442. https://doi.org/10.3390/rs13030442.

Rollins, M.G., Keane, R.E., Parsons, R.A., 2004. Mapping fuels and fire regimes using remote sensing, ecosystem simulation, and gradient modeling. Ecol. Appl. 14 (1), 75–95. https://doi.org/10.1890/02-5145.

Salis, M., Arca, B., Del Giudice, L., Palaiologou, P., Alcasena-Urdiroz, F., Ager, A., Fiori, M., Pellizzaro, G., Scarpa, C., Schirru, M., Ventura, A., Casula, M., Duce, P., 2021. Application of simulation modeling for wildfire exposure and transmission assessment in Sardinia, Italy. Int. J. Disaster Risk Reduc. 58, 102189 https://doi.org/10.1016/j.ijdrr.2021.102189.

Scott, J.H., Burgan, R.E., 2005. Standard Fire Behavior Fuel Models: A Comprehensive Set for Use with Rothermel's Surface Fire Spread Model (RMRS-GTR-153). U.S. Department of Agriculture, Forest Service, Rocky Mountain Research Station. https://doi.org/10.2737/RMRS-GTR-153.

Shendryk, Y., 2022. Fusing GEDI with earth observation data for large area aboveground biomass mapping. Int. J. Appl. Earth Obs. Geoinf. 115, 103108 https://doi.org/10.1016/j.jag.2022.103108.

Stefanidou, A., Gitas, I., Korhonen, L., Stavrakoudis, D., Georgopoulos, N., 2020a. LiDAR-Based Estimates of Canopy Base Height for a Dense Uneven-Aged Structured Forest. Rem. Sens. 12 (10), 1565. https://doi.org/10.3390/rs12101565.

Stefanidou, A., Gitas, I.Z., Katagis, T., 2020b. A national fuel type mapping method improvement using sentinel-2 satellite data. Geocarto Int. 1–21. https://doi.org/10.1080/10106049.2020.1756460.

Wang, C., Elmore, A.J., Numata, I., Cochrane, M.A., Lei, S., Hakkenberg, C.R., Li, Y., Zhao, Y., Tian, Y., 2022. A Framework for Improving Wall-to-Wall Canopy Height Mapping by Integrating GEDI LiDAR. Rem. Sens. 14 (15), 3618. https://doi.org/10.3390/rs14153618.

Wilkes, P., Jones, S., Suarez, L., Mellor, A., Woodgate, W., Soto-Berelov, M., Haywood, A., Skidmore, A., 2015. Mapping Forest Canopy Height Across Large Areas by Upscaling ALS Estimates with Freely Available Satellite Data. Rem. Sens. 7 (9), 12563–12587. https://doi.org/10.3390/rs70912563.

Wilson, B.T., Knight, J.F., McRoberts, R.E., 2018. Harmonic regression of Landsat time series for modeling attributes from national forest inventory data. ISPRS J. Photogrammetry Remote Sens. 137, 29–46. https://doi.org/10.1016/j.isprsjprs.2018.01.006.

Zhu, Z., 2017. Change detection using landsat time series: A review of frequencies, preprocessing, algorithms, and applications. ISPRS J. Photogrammetry Remote Sens. 130, 370–384. https://doi.org/10.1016/j.isprsjprs.2017.06.013.

Zhu, Z., Woodcock, C.E., 2014. Continuous change detection and classification of land cover using all available Landsat data. Remote Sens. Environ. 144, 152–171. https://doi.org/10.1016/j.rse.2014.01.011.